THE JOURNAL OF PHYSICAL CHEMISTRY A

Article

pubs.acs.org/JPCA

Initial Processes of Proton Transfer in Salicylideneaniline Studied by Time-Resolved Photoelectron Spectroscopy

Taro Sekikawa,*[,†,‡] Oliver Schalk,[†,§,∥] Guorong Wu,[†,⊥] Andrey E. Boguslavskiy,[†] and Albert Stolow[†]

[†]National Research Council Canada, 100 Sussex Drive, Ottawa, Ontario K1A 0R6, Canada

[‡]Department of Applied Physics, Hokkaido University, Kita-13 Nishi-8, Kita-ku, Sapporo 060-8628, Japan

[§]Stockholm University, Alba Nova University Center, Roslagstullsbacken 21, SE-10691 Stockholm, Sweden

[∥]Lehrstuhl für BioMolekulare Optik, Ludwig-Maximilians-Universität, Oettingenstraße 67, 80538 München, Germany

[⊥]State Key Laboratory of Molecular Reaction Dynamics, Dalian Institute of Chemical Physics, Chinese Academy of Sciences, Dalian, Liaoning 116023, P. R. China

ABSTRACT: Excited-state intramolecular proton transfer (ESIPT) in salicylideneaniline (SA) and selected derivatives substituted in the para position of the anilino group have been investigated by femtosecond time-resolved photoelectron spectroscopy (TRPES) and time-dependent density functional theory (TDDFT). SA has a twisted structure at the energetic minimum of the ground state, but ESIPT is assumed to take place through a planar structure, although this has not been fully established. The TRPES studies revealed that the excited-state dynamics within the S_1 band varied significantly with excitation wavelength. At finite temperatures, the ground state was found to sample a broad range of torsional angles, from planar to twisted. At lower photon energies (370 nm), only the planar ground-state molecules were excited, and the excited-state reaction took place within 50 fs. At higher energies (350 and 330 nm), predominantly twisted ground-state molecules were excited: they had to planarize before ESIPT could occur. This process was found to be slower in methylated SA but did not change significantly in the brominated and nitrated SAs. These substitution effects on the decay dynamics can be explained by modifications of the potential barriers, as predicted by the TDDFT calculations, and support the mechanism of a twisting motion of the anilino ring prior to ESIPT. The contribution of another pathway leading to internal conversion within the enol form was found to be minor at the excitation wavelengths considered here.

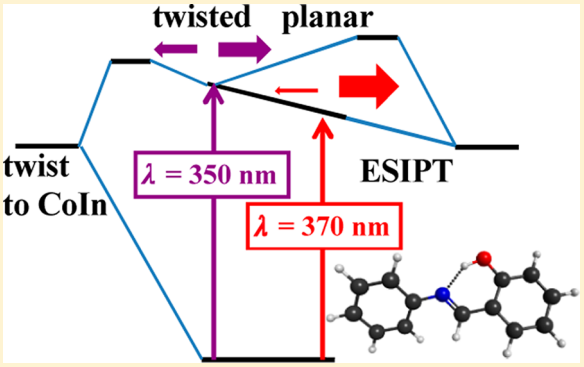

1. INTRODUCTION

Proton transfer is a fundamental and important chemical process of relevance to many biological systems.[1,2] One example is excited-state intramolecular proton transfer (ESIPT) in hydrogen-bonded systems. Because ESIPT can be initiated by ultrashort laser pulses, one can probe its dynamics in real time by time-resolved spectroscopy.[3−6] Among many systems containing an intramolecular hydrogen bond, *N*-salicylideneaniline (SA), shown in Figure 1a, is one of the most extensively studied, not only by static methods such as X-ray and ultraviolet−visible absorption spectroscopies before and after irradiation of the samples,[7−10] but also by time-resolved methods such as transient absorption,[11−17] fluorescence up-conversion,[12,18−22] infrared spectroscopy,[23] resonance-enhanced multiphoton ionization (REMPI) spectroscopy,[24] and time-resolved mass spectrometry[17] to trace the time evolution of the system. One of the reasons for this interest in SA is its change in color upon irradiation with ultraviolet (UV) light and thermal heating, known as photochromism and thermochromism, respectively.[25,26] Yet another reason is its applicability to optical storage and optical switch problems.[27]

Although various relaxation processes have been proposed, a consensus view of ESIPT in SA is schematically shown in Figure 1b: In the ground state, the enol form is the most stable conformation. In the excited state, however, the keto form is favored. Thus, upon absorption of a UV photon, the proton migrates from the hydroxy group to the nitrogen. In the keto form, cis−trans isomerization takes place, producing the photochromic product, namely, the trans-keto form, which is metastable in the ground state and can thermally transform back to the enol form.

Extensive research has revealed that, in addition to ESIPT, the twisting motions of the anilino and phenyl rings are important relaxation pathways in excited SA.[9,14−17,22,24,28,29] Theory predicts a ground-state torsion angle of 36° about the anil twist angle α ($C_7NC_6C_5$ dihedral angle; see Figure 1c for a definition of the critical angles considered in this study) at the B3LYP/6-31G* level of theory[28] and 44° at the HF/6-31G*

Received: February 14, 2013
Revised: March 15, 2013
Published: March 15, 2013

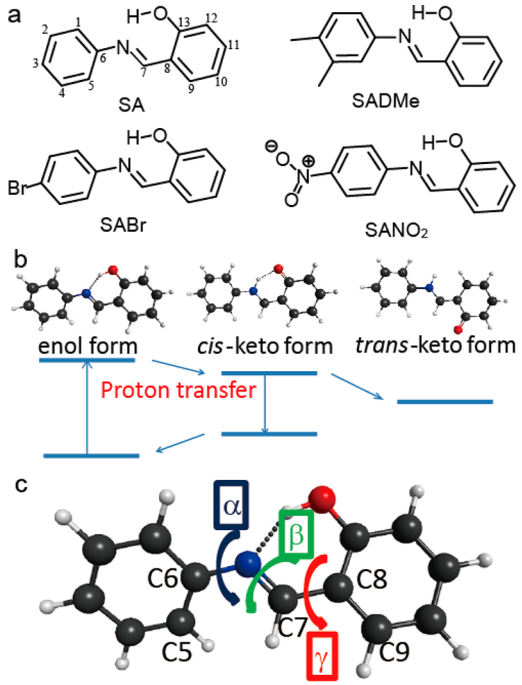

Figure 1. (a) Structures of *N*-salicylideneaniline (SA) and its derivatives, *N*-salicylidne-*p*-bromoanil (SABr), *N*-salicylidne-3,4-dimethylanil (SADMe), and *N*-salicylidne-*p*-nitroanil ($SANO_2$). (b) Simplified reaction scheme illustrating the processes under discussion. (c) Ground-state minimum structure of SA. Three twisting motions are critical in the excited-state dynamics of the molecule: Angles α, β, and γ are for twists about the anil group ($C_5C_6NC_7$), the central CN bond ($C_6NC_7C_8$), the phenol group ($NC_7C_8C_9$), respectively. In the ground state, the molecule is twisted by 35° about the anil group.

level.[29] An angle of 49° was found by X-ray diffraction of crystalline SA.[30,31] ESIPT, however, is considered to take place in planar molecules[28,29] only. The implications of a twisting motion being relevant to ESIPT have not been discussed thus far, despite extensive investigations of this molecule. A second relaxation pathway avoiding ESIPT was found and involves a 90° twist about the central CN bond β ($C_8C_7NC_6$ dihedral angle; see Figure 1c). This path might proceed through an intermediate $n\pi^*$ state,[29] although more recent work predicts a direct conversion to the ground state through a conical intersection (CI).[28] The conversion rate of this process is claimed to be on the order of that of ESIPT, rendering it a competing process.[28,29] Most experimental results can be understood in terms of this picture.[9,15−17,24,32] For example, REMPI experiments showed a relaxation of the S_1 state of the enol form within less than a few hundred femtoseconds,[24] which was explained by the two processes taking place in parallel. Similar studies with a higher time resolution but excitation to a higher-lying state claimed the dynamics to occur within 100 fs.[16,17] As both relaxation pathways involve twisting motions of anilino or phenyl rings, it is difficult to experimentally differentiate between the two reaction channels.

The differing behaviors of planar and twisted geometries in excited states have an analogy with thermochromic and photochromic SA derivatives in the solid state.[26,30,33,34] Thermochromic SAs have planar structures and energy differences between the enol and keto forms in the ground state that are small enough to permit thermal proton transfer. By contrast, photochromic SAs are nonplanar and do not show thermochromism because of their larger enol−keto energy gap in the ground state. By analogy with the dramatic change of the potential surface for proton transfer with respect to the ground-state twist angle, we argue here that the twist angle also affects the excited-state dynamics and plays a crucial role in ESIPT.

In the present study, we used time-resolved photoelectron spectroscopy (TRPES)[35] to study the dynamics of the isolated molecule, removing the influence of the solvent on rotational and torsional motions. In addition, TRPES allows for a direct comparison of experimental results with ab initio calculations because it is a sensitive and direct measure of both nuclear motion and evolving electronic character. TRPES was previously applied to the study of ESIPT in *o*-hydroxybenzaldehyde (OHBA).[4]

Here, we show that the excited-state relaxation dynamics depends not only on the excitation wavelength but also on specific substitutions in the para position of the anilino ring which influence the dynamics through inductive (I) and mesomeric (M) effects on the conjugated π system. In total, four different molecules were studied: SA, *N*-salicylidene-*p*-bromoanil (SABr), *N*-salicylidene-3,4-dimethylanil (SADMe), and *N*-salicylidene-*p*-nitroanil ($SANO_2$) (see Figure 1a for the structures). Finally, we considered our experimental results in terms of their associated potential surfaces, as obtained by time-dependent density functional theory (TDDFT).

2. EXPERIMENTAL AND THEORETICAL METHODS

SA, SABr, SADMe, and $SANO_2$ were obtained from MP Biomedicals and used without further purification. Sample molecules were seeded in helium at a stagnation pressure of 3 bar, heated to 333 K, and expanded into vacuum using an Even Lavie pulsed valve (200-μm diameter, conical nozzle), forming a skimmed supersonic molecular beam. TRPES experiments were performed as follows: The output of a Ti:sapphire laser (Legend, Coherent) was split into two beams. One was used to pump an optical parametric amplifier (OPA) (TOPAS, Light Conversion), the signal output of which was frequency quadrupled in nonlinear crystals to generate pump laser wavelengths of 370, 350, and 330 nm. The other beam was frequency doubled to generate 400-nm pulses, used for the probe. The pulse energies of the pump and probe pulses were about 2 and 20 μJ, respectively. The pulses were collinear and copropagating and loosely focused (f/100) into the interaction region of the photoelectron spectrometer, where it crossed the skimmed molecular beam. The relative laser polarization between pump and probe was set to the magic angle. The time delay between the pump and probe pulses was controlled by a motorized delay stage. The temporal resolution was about 150 fs, depending on the pump wavelength, and was determined by cross-correlation in 1,3-butadiene. The angle-integrated kinetic energy distributions of the ejected photoelectrons were recorded with a magnetic bottle time-of-flight photoelectron spectrometer.

Ground-state geometries and frequencies of the enol forms of SA, SABr, SADMe, and $SANO_2$ were optimized at the B3-LYP/6-31G* level using the GAMESS package.[36,37] Geometries for the rotation of the anilino group were calculated using the same method by fixing the $C_7NC_6C_5$ dihedral angle (see Figure 1). These geometries were used to obtain a potential energy surface and the oscillator strengths along the twist coordinate using B3LYP/aug-cc-pVDZ as implemented in the Turbomole code.[38−40] Linear interpolated paths between the optimized Franck−Condon point at a given (fixed) dihedral angle and the keto form, deduced from the keto minimum

dx.doi.org/10.1021/jp4016036 | J. Phys. Chem. A 2013, 117, 2971−2979

geometry in S_1 given by Ortiz-Sánchez et al.,[28] were also calculated. For the twisted geometries, we manually rotated the anilino group and optimized the structures with a fixed dihedral angle in the ground state. The same procedures were followed for the substituted molecules and for twists about the other dihedral angles depicted in Figure 1c.

3. RESULTS

3.1. Potential Energy Surfaces and ESIPT. In Figure 2, the ground-state energy along the anil twist angle α is shown

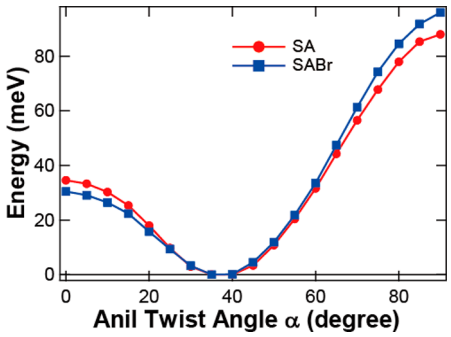

Figure 2. Calculated ground-state energies of *N*-salicylideneaniline (circles) and *N*-salicylidne-*p*-bromoanil (squares) as a function of the $C_7NC_6C_5$ dihedral angle (MP2/cc-pVDZ).

for SA and SABr as examples. This energy exhibits a minimum at 35°, but the dependence on the twist angle is less than 40 meV for angles up to 60° (MP2/cc-pVDZ). This means that, at the vibrational temperatures of the molecules in our molecular beam (estimated to be around 200 K, as vibrational cooling is not as efficient as rotational cooling), there is a finite probability of molecules achieving a broad range of anil twist angles. For example, at 200 K, the probability of finding molecules with anil twist angles between 0° and 15° is about 22%, assuming a Boltzmann distribution.

The solid squares and triangles in the left panels of Figure 3 show the energy levels of the S_1 and S_2 states of the enol forms as a function of the anil twist angle α (B3LYP/cc-pVDZ). From the energy curve, the planar structures were found to be the S_1 energetic minimum for all SA derivatives, in contrast to the ground state. Upon twisting, the S_1 potential energy surface rises significantly such that, at the red edge of the absorption spectrum, only the smaller population of planar ground-state molecules can be optically excited, whereas at the band center, the majority of the twisted ground-state molecules are predominantly excited. In this sense, 370-nm photons mainly excite planar SA, whereas 330-nm photons are mainly absorbed by twisted molecules. This heterogeneous behavior also explains the broad, structureless absorption spectrum (see section 3.2), which might otherwise be thought an indicator of very fast dynamics. At the same time, the oscillator strength of the $S_1 \leftarrow S_0$ transition depends critically on the twist angle, shown by the solid circles in the left panels of Figure 3: The oscillator strength has a maximum around 0°, decreases rapidly at a twist angle of about 60°, and almost vanishes at 90°. This favors the contributions of the planar ground-state fraction to the red edge of the absorption spectrum.

The right panels of Figure 3 show the linearly interpolated energy paths for ESIPT between the enol and keto forms in SA and its derivatives at different anil twist angles. For all angles and molecules, the S_1 state of the keto form lies below the S_1

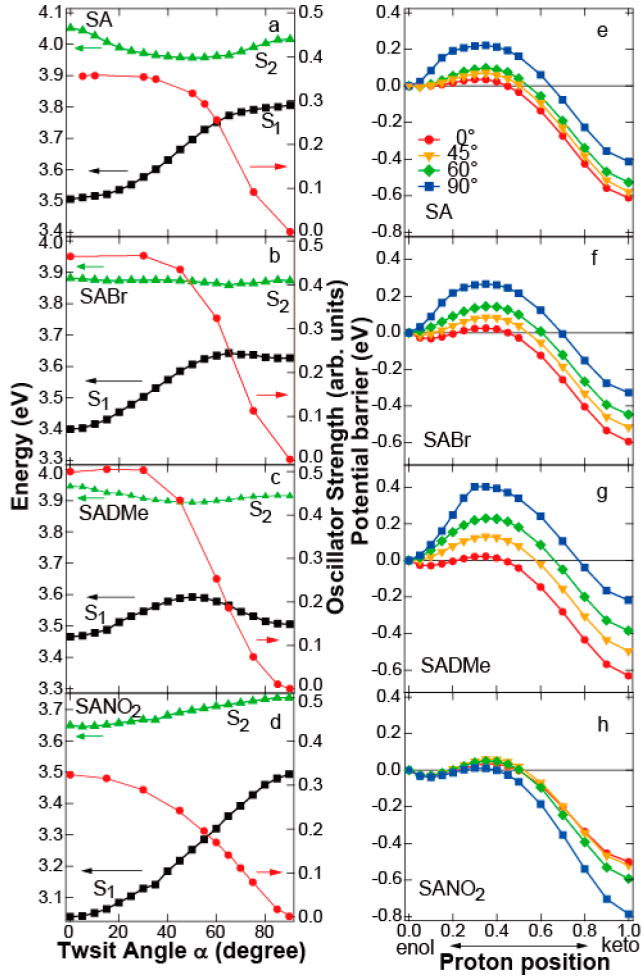

Figure 3. (Left) Potential energy curves of the S_1 (black squares) and S_2 (green triangles) states of the enol tautomer and oscillator strengths (red circles) of the $S_1 \leftarrow S_0$ transition as a function of $C_7NC_6C_5$ dihedral angle for (a) *N*-salicylideneaniline (SA), (b) *N*-salicylidne-*p*-bromoanil (SABr), (c) *N*-salicylidne-3,4-dimethylanil (SADMe), and (d) *N*-salicylidne-*p*-nitroanil ($SANO_2$). (Right) Potential energy curves as a function of the ESIPT reaction coordinate for (e) SA, (f) SABr, (g) SADMe, and (h) $SANO_2$. Circles, triangles, diamonds, and squares indicate the potential curves of $C_7NC_6C_5$ at dihedral angles with 0°, 45°, 60°, and 90°, respectively. It can be seen that the degree of variation of the barrier height with torsional angle depends strongly on the substituent.

state of the enol form, making ESIPT an energetically favorable process. However, a potential barrier separates the enol from the keto form, with the barrier increasing with increasing α. Therefore, it might be suspected that planarization should precede ESIPT. We propose, based on the differences between photochromic and thermochromic SAs,[34] that the anil twist angle α is one of the key parameters governing proton transfer in SA.

Comparing the energy curves of the SA derivatives with those of SA, we draw attention to the following two features: (1) Although the S_1 states of all the SA derivatives investigated in this work have a minimum at 0°, SADMe has a local minimum at 90°. As a result, pump photons might excite two types of molecules having different twist angles. This suggests that twisted SADMe might not necessarily relax to a planar structure upon photoexcitation. However, since the oscillator strength for larger twist angles decreases dramatically, we

dx.doi.org/10.1021/jp4016036 | J. Phys. Chem. A 2013, 117, 2971−2979

expect that the majority of excited molecules involve the planar configurations. Nevertheless, at this point, we cannot rule out the possibility that the decay dynamics in SADMe might differ from those of the others. (2) The barrier heights for ESIPT in SABr and SADMe are slightly higher than those of SA at the same twist angle. By contrast, the barrier height of $SANO_2$ is comparable to that of SA at twist angles less than 60°. This suggests that ESIPT will be forced to take place in SABr and SADMe at smaller twist angles than in SA and $SANO_2$. However, because of their higher barriers at a given twist angle, ESIPT is expected to be slower for the substituted species than for SA itself.

Aside from the anil twist angle α, two additional twist angles can be considered to play important roles in the excited-state dynamics of SA, namely, the CN twist angle β and the phenol twist angle γ (see Figure 1c). In both cases, we calculated the S_1 and S_2 potential energy curves along the respective twist axes. In the case of the phenol twist, the two states have increasing energies. However, following the CN twist (see Figure 4), we found a repulsive potential on S_1. This twist coordinate was previously found to be the relaxation path competing with ESIPT.[17,28]

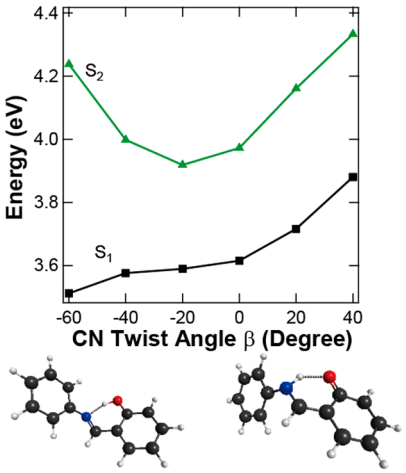

Figure 4. Potential energy curves of the S_1 (black squares) and S_2 (green triangles) states of the enol form as a function of the CN twist angle β. The insets show the molecular structures at $\beta = -60°$ (left) and $\beta = 40°$ (right).

3.2. Absorption Spectra. Figure 5 shows the absorption spectra of SA, SABr, SADMe, and $SANO_2$ recorded in heptane at room temperature. Since heptane is a nonpolar solvent, the basic features of the absorption spectra should be very close to those of the gas phase except for a red shift caused by solvation. SA, SABr, and SADMe have very similar absorption spectra, with a first maximum peaking around 350 nm. The absorption spectrum of $SANO_2$ extends to longer wavelengths. These absorption bands are attributed to the S_1 state of the enol form.[41] The arrows in Figure 5 indicate the excitation (pump) wavelengths used in our TRPES experiments. Note that the transition to the S_1 state is shifted toward the blue in the gas phase.

From the results of the TDDFT calculations shown in Figure 3, we assign two peaks around 350 and 320 nm in SA, SABr, and SADMe to transitions to the S_1 and S_2 states of the enol form. In the case of $SANO_2$, these peaks are shifted to 360 and 310 nm, respectively, but remain assigned to the same states. In

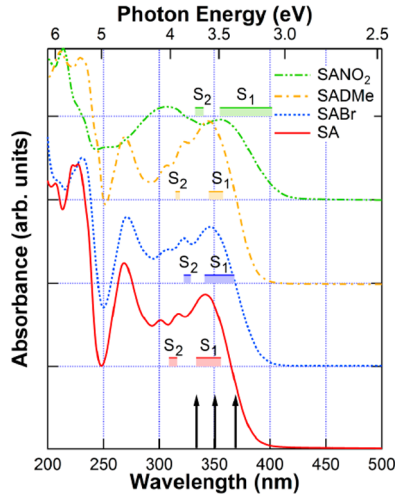

Figure 5. Absorption spectra of *N*-salicylideneaniline (SA, solid line), *N*-salicylidne-*p*-bromoanil (SABr, dotted line), *N*-salicylidne-3,4-dimethylanil (SADMe, dash-dotted line), and *N*-salicylidne-*p*-nitroanil ($SANO_2$, dash-double-dotted line) recorded in heptane. The baselines are shifted vertically for clarity. The hatched band on each baseline is the absorption band to the S_1 and S_2 states predicted by the theoretical calculations, taking into account the dependence of the energy on the $C_7NC_6C_5$ dihedral angle. The arrows indicate the pump energies used in time-resolved photoelectron spectroscopy. It is expected that the gas-phase spectra are slightly blue-shifted with respect to these.

the present experiments, we believe that the S_1 state was excited even at 330 nm, with the possible exception being $SANO_2$. The substituents have different I and M effects on the electronic states of the molecules. Bromine exhibits a −I effect and a +M effect; hence, it back-donates electrons accepted by the σ bond through its π orbital although, in total, bromine is considered to deactivate the aromatic ring as compared to hydrogen. The methyl groups have a weak +I effect. Thus, these two derivatives might have little effect on the electronic structures, resulting in almost identical absorption spectra compared to that of SA, except for a slight red shift. The nitro group exerts strong −I and −M effects and will decrease the electron density in the π system and, therefore, also on the anilino nitrogen, which is the accepting atom for the migrating hydrogen. Our calculations support this conclusion, predicting that the lowest unoccupied molecular orbital (LUMO) extends farther into the anilino ring, thus shifting the absorption spectrum of $SANO_2$ to longer wavelengths.

3.3. Time-Resolved Photoelectron Spectra. In panels a−c of Figure 6 are shown the two-dimensional time-resolved photoelectron spectra of SA pumped at 370, 350, and 330 nm, respectively, and probed with two photons of 400 nm. Time constants and their decay-associated photoelectron spectra were determined by a standard Levenberg−Marquardt global fitting routine over all electron kinetic energies and all time delays, wherein the two-dimensional data $S(E,\Delta t)$ are expressed as

$$S(E, \Delta t) = \sum_i A_i(E)\, P_i(\Delta t) \otimes g(\Delta t) \quad (1)$$

where $A_i(E)$ is the decay-associated photoelectron spectrum of the ith channel having a time-dependent population $P_i(\Delta t)$, and $g(\Delta t)$ is the experimentally determined Gaussian cross-correlation function. For details, see ref 42. Panels d−f of Figure 6 show the time dependence of the photoelectron yield

dx.doi.org/10.1021/jp4016036 | J. Phys. Chem. A 2013, 117, 2971−2979

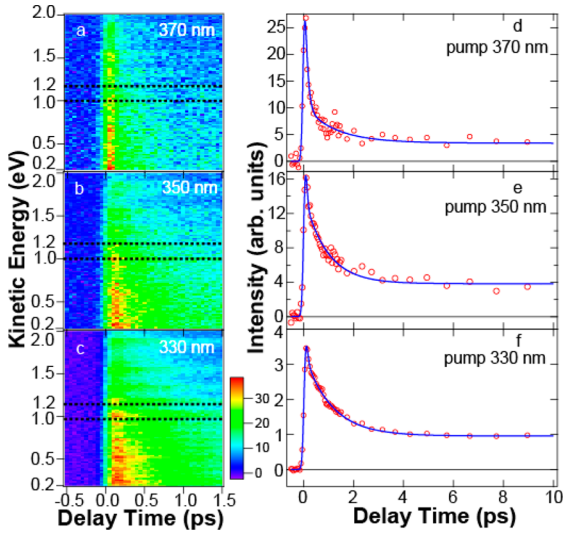

Figure 6. Time-resolved photoelectron spectra of *N*-salicylideneaniline at pump wavelengths of (a) 370, (b) 350, and (c) 330 nm. The probe wavelength was 400 nm in all cases. The decay-associated spectra (Figure 7) result from two-dimensional fits to these data. Time traces integrated over the energy range of 1.0−1.2 eV are shown in the right panel for each excitation wavelength.

in the range of 1.0−1.2 eV, excited at 370, 350, and 330 nm, respectively. With decreasing excitation wavelength, the decay lifetime appears to be longer. This same trend was observed for all derivatives.

In the fitting procedure, at least three exponential functions were nontrivially required to represent the data of all molecules sufficiently well. Here, the longest lifetime, τ_3, was set to 10 μs, because the photoelectron yield after 10 ps was almost constant up to 500 ps. The other time constants are listed in Table 1.

Table 1. Decay Lifetimes[a]

		pump photon energy		
		3.35 eV (370 nm)	3.54 eV (350 nm)	3.76 eV (330 nm)
SA	τ_1 (fs)	50 ± 20	40 ± 20	45 ± 20
	τ_2 (ps)	0.97 ± 0.10	1.17 ± 0.10	1.08 ± 0.10
SABr	τ_1 (fs)	45 ± 20	60 ± 20	70 ± 20
	τ_2 (ps)	1.00 ± 0.10	1.35 ± 0.10	0.70 ± 0.10
SADMe	τ_1 (fs)	60 ± 20	280 ± 20	290 ± 50
	τ_2 (ps)	0.80 ± 0.30	3.20 ± 0.30	1.10 ± 0.30
$SANO_2$	τ_1 (fs)	23 ± 13	70 ± 20	60 ± 20
	τ_2 (ps)	1.03 ± 0.29	1.40 ± 0.30	0.76 ± 0.30

[a] τ_3 was fixed at 10 μs.

For all measurements, we found a fast decay τ_1, often within 100 fs, and a medium time constant τ_2 between 0.7 and 1.5 ps. Their variation is discussed in the following section. The most significant difference between the measurements, however, is seen in the form of the decay-associated spectrum (DAS) as a function of pump wavelength, as shown in Figure 7. (In the case of 370-nm excitation, the signal-to-noise ratios for SADMe and $SANO_2$ were too poor to warrant presentation.) The ordinates are normalized with respect to the DAS of τ_3. As shown in panels c, f, i, and l of Figure 7, these spectra are broad and rising toward lower electron kinetic energies in all experiments. The apparent lack of structure might indicate a vibrationally hot molecule, as can be the case for a long-lived

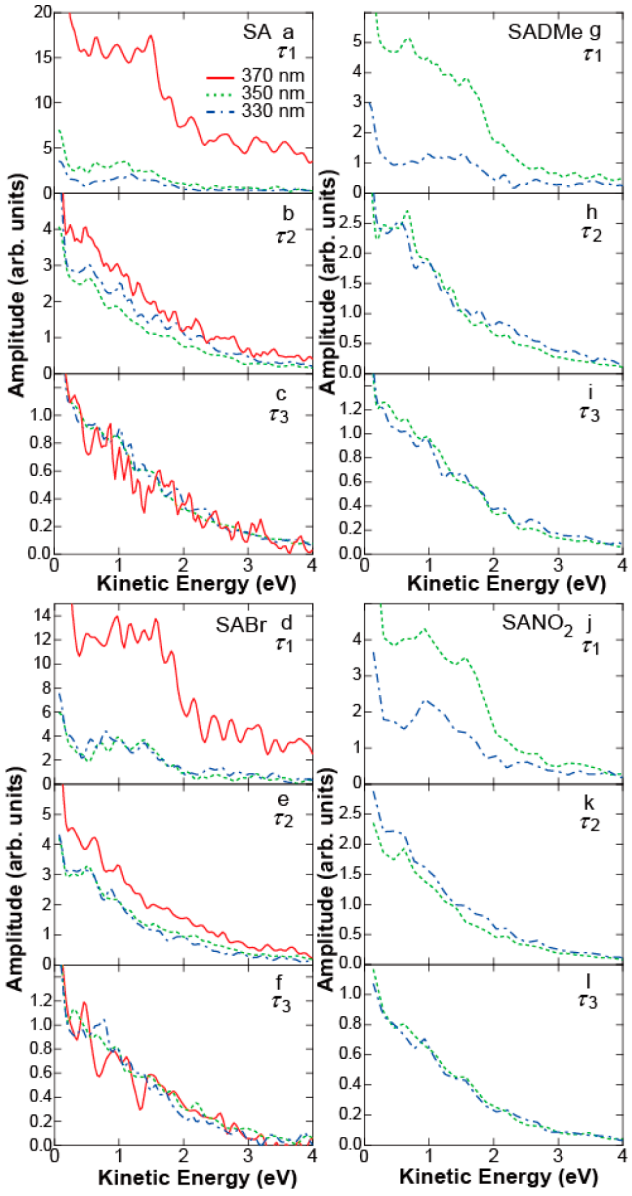

Figure 7. Decay-associated spectra (DAS) for τ_1, τ_2, and τ_3 time constants of *N*-salicylideneaniline (SA, a−c), *N*-salicylidne-*p*-bromoanil (SABr, d−f), *N*-salicylidne-3,4-dimethylanil (SADMe, g−i), and *N*-salicylidne-*p*-nitroanil ($SANO_2$, j−l), pumped at 370 nm (solid line), 350 nm (dotted line), and 330 nm (dash-dotted line). DAS of SADMe and $SANO_2$ pumped at 370 nm are not shown because of poor signal-to-noise ratios. In each case, the amplitudes of the τ_1 and τ_2 DAS spectra were normalized to that of τ_3. It can be seen that the relative amplitude of the τ_1 DAS decreases with increasing excitation energy.

lower-lying state. (See, for example, the longest-time-constant DAS of cyclohexene in ref 43.) In Figure 7a, it is seen that the fast time constant in SA has distinctively larger amplitude at 370 nm than at 350 and 330 nm (factor of 5:1−10:1). The same is true for SABr (Figure 7d) but with a smaller ratio (3:1). For SADMe and $SANO_2$, shown in panels g and j of Figure 7, we also observe a difference between the 330- and 350-nm results, where the τ_1 amplitude is 3 times larger at 350 nm.

4. DISCUSSION

4.1. Decay Dynamics of SA. At a pump wavelength of 370 nm (3.35 eV, see Figure 3a), we predominantly excited the S_1

dx.doi.org/10.1021/jp4016036 | J. Phys. Chem. A 2013, 117, 2971−2979

state in its planar form. As a consequence, the ESIPT channel can be accessed without a barrier for most excited molecules. We note that τ_1 has the largest amplitude in the DAS. This allows the ESIPT process to be attributed to this time constant.

At pump wavelengths of 350 and 330 nm, the relative amplitude of the DAS related to τ_1 is significantly reduced. This signifies that a smaller percentage of the molecules undergo a prompt proton transfer, which can be rationalized by the calculated energy curves in Figure 3: Here, molecules are excited at a finite anil twist angle, leading to a rise in the energy barrier for the ESIPT pathway. This barrier enforces planarization to take place first and delays the ESIPT channel. This process is schematically illustrated in Figure 8, where the

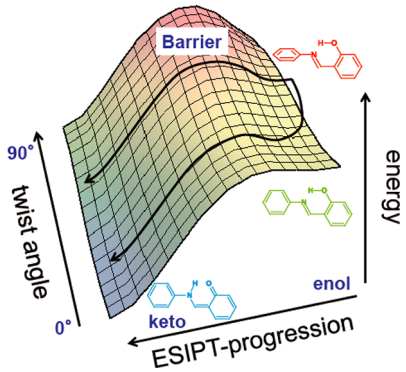

Figure 8. Schematic illustration of a potential surface for the S_1 state of *N*-salicylideneaniline as a function of twist angle and proton coordinate. The barrier to excited-state intramolecular proton transfer (ESIPT) decreases as planarity is approached, suggesting that twisting should precede ESIPT.

two-dimensional dependence of the energy surface of the S_1 state on the twist angle and interpolated reaction path is plotted. Unless the initial motion is along the proton-transfer coordinate, the trajectories are likely to follow the gradients in the excited state. One of these gradients is along the planarization coordinate, leading to ESIPT.

At least one other gradient leads the molecule away from the Franck–Condon region. This gradient points along the CN twist toward an internal conversion within the enol form (see the Introduction), opening a channel that competes directly with ESIPT. The study by Ortiz-Sánchez et al.[28] and our calculation shown in Figure 4 predict that there is no barrier on the potential energy surface along the CN twist coordinate. However, based on energetic arguments, a steep barrierless gradient leading directly toward the CN twist channel is in disagreement with experimental findings, because the absence of a barrier should cause dynamics to almost exclusively follow this reaction path. In consequence, direct relaxation back to the ground state of the enol form would be the dominant relaxation pathway, given the barrier for the competing ESIPT process. However, the ESIPT product was confirmed by vibrational spectroscopy,[11,23] and the time dependence of the various experiments would be hard to explain without invoking ESIPT.[13−15,17,22] Therefore, we assume that there must be at least a small barrier in the relaxation processes involving the CN twist, or that other effects such as conical intersection topography significantly affect these dynamics. The phenomenological evidence indicates that ESIPT is primarily responsible for the fast relaxation. Evidence that the ESIPT channel is indeed the major one was obtained by studying substituent effects (see section 4.2).

It is worth noting that, based on our experiments on SA alone, we cannot unambiguously distinguish between the two relaxation paths because the two channels have similar photoelectron spectra. Therefore, $1/\tau_2$ is the sum of the rates of the two competing processes: twisting motion prior to ESIPT and rotational motion prior to internal conversion.

The DAS of the long-lived τ_3 component, shown in Figure 7, is less structured than the spectra of τ_1 and τ_2, and therefore, it likely originates from another excited state. The only known state in SA that is energetically accessible is the excited keto form. The rise of this DAS toward lower photoelectron kinetic energies is consistent with a lower-lying state with much internal energy distributed in vibrational modes. (Note that the broad spectra are partly governed by ionization through Rydberg states, as was observed in earlier studies.[44,45]) We do not see any indication of a return to the ground state through cis–trans isomerization to the trans-keto form, at least within the 500-ps range of our experiments. However, in section 4.3, we present an alternative interpretation.

4.2. Substitution Effects. To extract a more complete picture of the proton-transfer process and the effects that might govern ESIPT dynamics, we investigated the influence of the substituents on the SA dynamics. As discussed, the substituents modify the potential energy surfaces mainly through I and M effects. In the following subsections, we discuss these effects referring to our TRPES data and the energy curves shown in Figures 3, 6, and 7.

4.2.1. SABr. In SABr, a bromine atom replaces a hydrogen atom in the para position of the anilino ring. This substitution has no inertial influence on the anil twist motion (i.e. planarization), but it should influence the CN twist motion that leads to the CI in the enol species because of the increased mass of the anil group. Bromine itself has a weak electron-withdrawing (−I) effect but back-donates electrons to the ring through the π bond (+M effect). In total, this is reflected in the barrier to ESIPT, which, at low moderate twist angles, is only slightly higher than in SA, and therefore, the mass effect is the most important factor here. The observed time constants are identical within experimental uncertainty. This is remarkable, because one would have expected τ_1 to increase if the CI pathway within the enol species were important. Hence, we conclude that this CI channel does not play a significant role in the fast relaxation step and that ESIPT is the dominant pathway at the excitation wavelengths employed here.

4.2.2. SADMe. SADMe has two methyl groups replacing the hydrogen in the para position and one of the hydrogens in the meta positions on the anilino ring. Methyl groups are weakly electron-donating through the σ bond (+I effect). Although these methyl substitutions might be considered to be electronically innocuous, they turn out to be important: (1) The second time constant τ_2 significantly increases for wavelengths shorter than 370 nm (see Table 1). (2) The potential barrier for ESIPT rises. (3) The S_1 potential energy surface exhibits a maximum at 50° before it decreases at larger twist angles (Figure 3c), which causes the gradient toward planarization to decrease concomitantly. In addition, the inertia for rotation about the anil twist angle is increased because of the substitution in the meta position. It is only at larger twist angles, that is, upon the decoupling of the π systems, that the methyl groups play a noteworthy role. As a consequence, the dynamics seen at a pump wavelength of 370 nm is comparable

dx.doi.org/10.1021/jp4016036 | J. Phys. Chem. A 2013, 117, 2971−2979

to the dynamics of the other molecules: the differences are observed only at higher excitation energies.

4.2.3. $SANO_2$. The nitro group is heavily withdrawing electrons through −I and −M effects, and both the theoretical and measured absorption spectra are red-shifted (see Figures 3 and 5). Moreover, the barrier for ESIPT is significantly decreased at large twist angles, which might be expected to impact the dynamics. In contrast, the TRPES spectra look very similar to the spectra of SA at all three wavelengths.

The unexpectedly small influence of the nitro group on the decay dynamics can be attributed to the small oscillator strength seen at large twist angles (Figure 3d). At twist angles less than 60°, the barrier heights within $SANO_2$ are comparable to those of SA, and the decay dynamics in $SANO_2$ is therefore similar to that in SA. In addition, the ESIPT coordinate seems not to be directly prepared upon excitation at higher pump energies because of the small oscillator strength. It seems that planarization must precede ESIPT. Note that, despite the absence of a large barrier, the potential remains quite flat until halfway through the proton-transfer reaction, likely leading to a somewhat slower dynamics.

4.3. Comparison with Previous Studies. Salicylideneaniline has been studied in the gas and liquid phases, and various relaxation pathways have been proposed. Sliwa and co-workers excited SA at 266 nm and studied the dynamics using time-resolved mass spectrometry and transient absorption in acetonitrile.[17] They developed a detailed pathway for the dynamics based on multiple time constants. One finding was that the quantum yields for the enol and twist channels depend on the excitation wavelength: ESIPT is the dominant channel upon excitation at 355 nm, and rotation about the CN bond is the major pathway after excitation with 266 nm. This agrees with our analysis in sections 4.1 and 4.2 and provides further evidence that a barrier exists in the CN twist path.

Ortiz-Sánchez and co-workers studied excited-state dynamics using TDDFT molecular dynamics.[28] They proposed that the enol pathway and ESIPT are associated with time constants of 38 and 50 fs, respectively. These time constants are in agreement with our measurements, although we suggest that the ESIPT pathway is dominant and relaxation along the CN twist pathway is suppressed (see section 4.2.1). Moreover, these authors did not consider the role of the anil twist angle in the SA ground state and its influence on the dynamics. Ortiz-Sánchez and co-workers further showed that the cis-keto state does not have a minimum on S_1 and, therefore, cis−trans isomerization would occur on fast time scales. This calculation suggests that the long-lived "final state" seen in our data could be the trans-keto ground state: This state would be expected to have a significant photoionization cross section, because it should be resonant with the probe pulse. We note that this scheme does not contradict our interpretation of the initial steps in the proton transfer dynamics: Our second time constant could easily convolve torsional dynamics in both the enol and keto forms, as the two processes are thought to occur on similar time scales.[14,22]

In addition to SA, ESIPT was studied in related species such as 2-(2′-hydroxyphenyl)benzothiazole (HBT) and 2-(2′-hydroxyphenyl)benzoxazole (HBO) in both the liquid[46−50] and gas[51] phases. However, in these molecules, the anilino group is fixed and cannot twist. Therefore, the molecules are already in an optimal geometry for ESIPT, corroborated by the direct observation of coherent vibrational oscillations in the excited state. Transient absorption experiments in the gas phase showed similar time constants.[51] In HBT, ESIPT was assigned to a sub-50-fs time constant, whereas a second time constant of 2.6 ps was suggested to originate from cis−trans isomerization followed by a return to the ground state in the keto form.[51] Aspects of this proposed mechanism might also apply to SA and in agreement with theoretical findings.[28] However, the dependence of τ_2 on the excitation wavelength and the large τ_1 DAS amplitude at 370 nm strongly suggest that the barrier to ESIPT in the excited enol state plays a significant role.

5. CONCLUSIONS

In conclusion, we studied excited-state intramolecular proton transfer (ESIPT) in salicylideneaniline (SA) and substituted species using time-resolved photoelectron spectroscopy (TRPES) and time-dependent density functional theory (TDDFT). An overview of the observed dynamics is shown in Figure 9: Planar ground-state geometries are preferentially excited at 370 nm, and ESIPT, benefitting from planarity, takes place within 50 fs. Upon excitation at shorter wavelengths, twisted ground-state molecules are preferentially excited and experience a potential barrier between the enol and keto forms of SA, thereby impeding proton transfer. Subsequent to ESIPT, cis−trans isomerization might occur on the picosecond time scale. In an alternative pathway, rotation about the central CN bond leads to relaxation within the enol form. According to our analysis, this path is minor upon excitation to S_1. Substitutions on the anilino ring mainly influenced the barrier height, and a correlation between the decay time of the signal and the height of this barrier was observed. A main conclusion is that the torsional dynamics in the excited state is a key aspect of ESIPT in SA. Future studies might consider TRPES studies of other SA derivatives to further elaborate on the role of torsional dynamics in ESIPT.

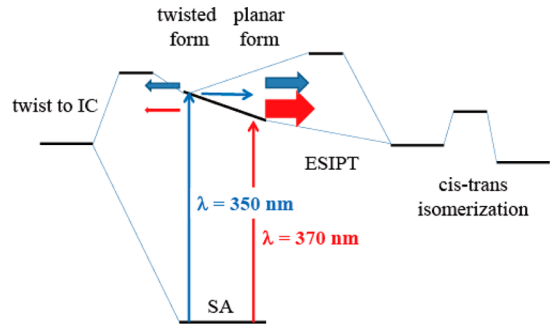

Figure 9. Proposed reaction scheme of *N*-salicylideneaniline upon photoexcitation with 370- and 350-nm photons. See text for details.

AUTHOR INFORMATION

Corresponding Author

*E-mail: sekikawa@eng.hokudai.ac.jp.

Notes

The authors declare no competing financial interest.

ACKNOWLEDGMENTS

T.S. was supported by a Grant-in-Aid for Excellent Young Researcher Overseas Visit Program and partially by a Grant-in-Aid for Scientific Research (B) (23340116) from the Japan Society for the Promotion of Science. O.S. thanks the Humboldt Foundation for a research fellowship. A.S. acknowledges financial support from the Natural Sciences and

Engineering Research Council (NSERC) of Canada's Discovery Grant program.

REFERENCES

(1) Paddock, M. L.; Rongey, S. H.; Feher, G.; Okamura, M. Y. Pathway of Proton Transfer in Bacterial Reaction Centers: Replacement of Glutamic Acid 212 in the L Subunit by Glutamine Inhibits Quinone (Secondary Acceptor) Turnover. *Proc. Natl. Acad. Sci. U.S.A.* **1989**, *86*, 6602−6606.

(2) Garczarek, F.; Gerwert, K. Functional Waters in Intraprotein Proton Transfer Monitored by FTIR Difference Spectroscopy. *Nature (London)* **2006**, *439*, 109−112.

(3) *Ultrafast Hydrogen Bonding Dynamics and Proton Transfer Processes in the Condensed Phase*; Elsaesser, T., Bakker, H. J., Eds.; Kluwer Academic Publishers: Dordrecht, The Netherlands, 2002.

(4) Lochbrunner, S.; Schultz, T.; Schmitt, M.; Shaffer, J. P.; Zgierski, M. Z.; Stolow, A. Dynamics of Excited-State Proton Transfer Systems via Time-Resolved Photoelectron Spectroscopy. *J. Chem. Phys.* **2001**, *114*, 2519−2522.

(5) Lochbrunner, S.; Stock, K.; Riedle, E. Direct Observation of the Nuclear Motion During Ultrafast Intramolecular Proton Transfer. *J. Mol. Struct.* **2004**, *700*, 13−18.

(6) Takeuchi, S.; Tahara, T. Coherent Nuclear Wavepacket Motions in Ultrafast Excited-State Intramolecular Proton Transfer: Sub-30-fs Resolved Pump−Probe Absorption Spectroscopy of 10-Hydroxybenzo[*h*]quinoline in Solution. *J. Phys. Chem. A* **2005**, *109*, 10199−10207.

(7) Rosenfeld, T.; Ottolenghi, M.; Meyer, A. Y. Photochromic Anils. Structure of Photoisomers and Thermal Relaxation Processes. *Mol. Photochem.* **1973**, *5*, 39−60.

(8) Harada, J.; Uekusa, H.; Ohashi, Y. X-ray Analysis of Structural Changes in Photochromic Salicylideneaniline Crystals. Solid-State Reaction Induced by Two-Photon Excitation. *J. Am. Chem. Soc.* **1999**, *121*, 5809−5810.

(9) Otsubo, N.; Okabe, C.; Mori, H.; Sakoda, K.; Amimoto, K.; Kawato, T.; Sekiya, H. Excited-State Intramolecular Proton Transfer in Photochromic Jet-Cooled *N*-Salicylideneaniline. *J. Photochem. Photobiol. A* **2002**, *154*, 33−39.

(10) Harada, J.; Fujiwara, T.; Ogawa, K. Crucial Role of Fluorescence in the Solid-State Thermochromism of Salicylideneanilines. *J. Am. Chem. Soc.* **2007**, *129*, 16216−16221.

(11) Nakagaki, R.; Kobayashi, T.; Nakamura, J.; Nagakura, S. Spectroscopic and Kinetic Studies of the Photochromism of *N*-Salicylideneanilines and Related Compounds. *Bull. Chem. Soc. Jpn.* **1977**, *50*, 1909−1912.

(12) Kownacki, K.; Mordzinski, A.; Wilbrandt, R.; Grabowska, A. Laser-Induced Absorption and Fluorescence Studies of Photochromic Schiff Bases. *Chem. Phys. Lett.* **1994**, *227*, 270−276.

(13) Mitra, S.; Tamai, N. Dynamics of Photochromism in Salicylideneaniline: A Femtosecond Spectroscopic Study. *Phys. Chem. Chem. Phys.* **2003**, *5*, 4647−4652.

(14) Ziółek, M.; Kubicki, J.; Maciejewski, A.; Naskręcki, R.; Grabowska, A. An Ultrafast Excited State Intramolecular Proton Transfer (ESIPT) and Photochromism of Salicylideneaniline (SA) and Its "Double" Analogue Salicylaldehyde Azine (SAA). A Controversial Case. *Phys. Chem. Chem. Phys.* **2004**, *6*, 4682−4689.

(15) Ziółek, M.; Burdziński, G.; Filipczak, K.; Karolczak, J.; Maciejewski, A. Spectroscopic and Photophysical Studies of the Hydroquinone Family of Photochromic Schiff Bases Analyzed over a 17-Orders-of-Magnitude Time Scale. *Phys. Chem. Chem. Phys.* **2008**, *10*, 1304−1318.

(16) Sliwa, M.; Mouton, N.; Ruckebusch, C.; Aloïse, S.; Poizat, O.; Buntinx, G.; Métivier, R.; Nakatani, K.; Masuhara, H.; Asahi, T. Comparative Investigation of Ultrafast Photoinduced Processes in Salicylideneaniline-Aminopyridine in Solution and Solid State. *J. Phys. Chem. C* **2009**, *113*, 11959−11968.

(17) Sliwa, M.; Mouton, N.; Ruckebusch, C.; Poisson, L.; Idrissi, A.; Aloïse, S.; Potier, L.; Dubois, J.; Poizat, O.; Buntinx, G. Investigation of Ultrafast Photoinduced Processes for Salicylidene Aniline in Solution and Gas Phase: Toward a General Photo-Dynamical Scheme. *Photochem. Photobiol. Sci.* **2010**, *9*, 661−669.

(18) Barbara, P. F.; Rentzepis, P. M.; Brus, L. E. Photochemical Kinetics of Salicylideneaniline. *J. Am. Chem. Soc.* **1980**, *102*, 2786−2791.

(19) Sekikawa, T.; Kobayashi, T.; Inabe, T. Femtosecond Fluorescence Study of the Substitution Effect on the Proton Transfer in Thermochromic Salicylideneaniline Crystals. *J. Phys. Chem. A* **1997**, *101*, 644−649.

(20) Sekikawa, T.; Kobayashi, T.; Inabe, T. Femtosecond Fluorescence Study of Proton-Transfer Process in Thermochromic Crystalline Salicylideneanilines. *J. Phys. Chem. B* **1997**, *101*, 10645−10652.

(21) Vargas, C. V. Time-Resolved Fluorescence of Salicylideneaniline Compounds in Solution. *J. Phys. Chem. A* **2004**, *108*, 281−288.

(22) Rodríguez-Córdoba, W.; Zugazagoitia, J. S.; Collado-Fregoso, E.; Peon, J. Excited State Intramolecular Proton Transfer in Schiff Bases. Decay of the Locally Excited Enol State Observed by Femtosecond Resolved Fluorescence. *J. Phys. Chem. A* **2007**, *111*, 6241−6247.

(23) Yuzawa, T.; Takahashi, H.; Hamaguchi, H. Submicrosecond Time-Resolved Infrared Study on the Structure of the Photoinduced Transient Species of Salicylideneaniline in Acetonitrile. *Chem. Phys. Lett.* **1993**, *202*, 221−226.

(24) Okabe, C.; Nakabayashi, T.; Inokuchi, Y.; Nishi, N.; Sekiya, H. Ultrafast Excited-State Dynamics in Photochromic *N*-Salicylideneaniline Studied by Femtosecond Time-Resolved REMPI Spectroscopy. *J. Chem. Phys.* **2004**, *121*, 9436−9442.

(25) *Photochromism: Molecules and Systems*; Dürr, H., Bouas-Laurent, H., Eds.; Elsevier B.V.: Amsterdam, 2003.

(26) Samat, A.; Lokshin, V. Thermochromism of Organic Compounds. In *Organic Photochromic and Thermochromic Compounds*; Crano, J. C., Guglielmetti, R. J., Eds.; Plenum Press: New York, 1998; Vol. *2*, pp 415−466.

(27) Irie, M. Photochromism: Memories and Switches—Introduction. *Chem. Rev.* **2000**, *100*, 1683−1684.

(28) Ortiz-Sánchez, J. M.; Gelabert, R.; Moreno, M.; Lluch, J. M. Electronic-Structure and Quantum Dynamical Study of the Photochromism of the Aromatic Schiff Base Salicylideneaniline. *J. Chem. Phys.* **2008**, *129* (214308), 1−11.

(29) Zgierski, M. Z.; Grabowska, A. Photochromism of Salicylideneaniline (SA). How the Photochromic Transient Is Created: A Theoretical Approach. *J. Chem. Phys.* **2000**, *112*, 6329−6337.

(30) Bergman, J.; Leiserowitz, L.; Osaki, K. 392. Topochemistry. Part X. The Crystal and Molecular Structures of 2-Chloro-*N*-salicylideneaniline. *J. Chem. Soc.* **1964**, 2086−2100.

(31) Destro, R.; Gavezzotti, A.; Simonetta, M. Salicylideneaniline. *Acta Crystallogr. B* **1978**, *34*, 2867−2869.

(32) Ziólek, M.; Burdzinski, G.; Douhal, A. Long-Living Structures of Photochromic Salicylaldehyde Azine: Polarity and Viscosity Effects from Nanoseconds to Hours. *Photochem. Photobiol. Sci.* **2012**, *11*, 1389−1400.

(33) Bergman, J.; Leiserowitz, L.; Schmidt, G. M. J. 391. Topochemistry. Part IX. The Crystal and Molecular Structures of *N*-5-Chlorosalicylideneaniline near 90 and 300 K. *J. Chem. Soc.* **1964**, 2068−2085.

(34) Cohen, M. D.; Schmidt, G. M. J. Photochromy and Thermochromy of Anils. *J. Phys. Chem.* **1962**, *66*, 2442−2446.

(35) Stolow, A.; Underwood, J. G. Time-Resolved Photoelectron Spectroscopy. *Adv. Chem. Phys.* **2008**, *139*, 497−583.

(36) Gordon, M. S.; Schmidt, M. W. Advances in Electronic Structure Theory: GAMESS a Decade Later. In *Theory and Applications of Computational Chemistry, the First Forty Years*; Dykstra, C. E., Frenking, G., Kim, K. S., Scuseria, G. E., Eds.; Elsevier: Amsterdam, 2005; pp 1167−1189.

(37) Schmidt, M. W.; Baldridge, K. K.; Boatz, J. A.; Elbert, S. T.; Gordon, M. S.; Jensen, J. H.; Koseki, S.; Matsunaga, N.; Nguyen, K. A.; Su, S. J.; Windus, T. L.; Dupuis, M.; Montgomery, J. A., Jr. General

Atomic and Molecular Electronic Structure System. *Comput. Chem.* **1993**, *14*, 1347−1363.
(38) Bauernschmitt, R.; Ahlrichs, R. Treatment of Electronic Excitations within the Adiabatic Approximation of Time Dependent Density Functional Theory. *Chem. Phys. Lett.* **1996**, *256*, 454−464.
(39) Bauernschmitt, R.; Ahlrichs, R. Stability Analysis for Solutions of the Closed Shell Kohn−Sham Equation. *J. Chem. Phys.* **1996**, *104*, 9047−9052.
(40) Furche, F.; Rappoport, D. Density Functional Methods for Excited States: Equilibrium Structure and Electronic Spectra. In *Theoretical and Computational Chemistry*; Olivucci, M., Ed.; Elsevier: Amsterdam, 2005; Vol. *16*.
(41) Morales, R., G. E.; Jara, G. P.; Vargas, V. Ultraviolet Absorption Bands and Electronic Charge Transfers of Salicylideneanilines in Singlet Excited States. *Spectrosc. Lett.* **2001**, *34*, 1−12.
(42) Schalk, O.; Boguslavskiy, A. E.; Stolow, A. Substituent Effects on Dynamics at Conical Intersections: Cyclopentadienes. *J. Phys. Chem. A* **2010**, *114*, 4058−4064.
(43) Schalk, O.; Boguslavskiy, A. E.; Stolow, A.; Schuurman, M. S. Through-Bond Interactions and the Localization of Excited-State Dynamics. *J. Am. Chem. Soc.* **2011**, *133*, 16451−16458.
(44) Brogaard, R. Y.; Boguslavskiy, A. E.; Schalk, O.; Enright, G. D.; Hopf, H.; Raev, V. A.; Jones, P. G.; Thomsen, D. L.; Sølling, T. I.; Stolow, A. Pseudo-Bimolecular [2 + 2] Cycloaddition Studied by Time-Resolved Photoelectron Spectroscopy. *Chem.—Eur. J.* **2011**, *17*, 3922−3931.
(45) Brogaard, R. Y.; Schalk, O.; Boguslavskiy, A. E.; Enright, G. D.; Hopf, H.; Raev, V.; Tarcoveanu, E.; Sølling, T. I.; Stolow, A. The Paternò−Büchi Reaction: Importance of Triplet States in the Excited-State Reaction Pathway. *Phys. Chem. Chem. Phys.* **2012**, *14*, 8572−8580.
(46) Lochbrunner, S.; Wurzer, A. J.; Riedle, E. Ultrafast Excited-State Proton Transfer and Subsequent Coherent Skeletal Motion of 2-(2′-Hydroxyphenyl)benzothiazole. *J. Chem. Phys.* **2000**, *112*, 10699−10702.
(47) Lochbrunner, S.; Wurzer, A. J.; Riedle, E. Microscopic Mechanism of Ultrafast Excited State Intramolecular Proton Transfer: A 30-fs Study of 2-(2′-Hydroxyphenyl)benzothiazole. *J. Phys. Chem. A* **2003**, *107*, 10580−10590.
(48) Schriever, C.; Barbatti, M.; Stock, K.; Aquino, A. L. J. A.; Tunega, D.; Lochbrunner, S.; Riedle, E.; Vivie-Riedle, R. D.; Lischka, H. The Interplay of Skeletal Deformations and Ultrafast Excited-State Intramolecular Proton Transfer: Experimental and Theoretical Investigation of 10-Hydroxybenzo[*h*]quinoline. *Chem. Phys.* **2008**, *347*, 446−461.
(49) Vivie-Riedle, R. D.; Waele, V. D.; Kurtz, L.; Riedle, E. Ultrafast Excited-State Proton Transfer of 2-(2′-Hydroxyphenyl)benzothiazole: Theoretical Analysis of the Skeletal Deformations and the Active Vibrational Modes. *J. Phys. Chem. A* **2003**, *107*, 10591−10599.
(50) Lee, J.; Kim, C. H.; Joo, T. Active Role of Proton in Excited State Intramolecular Proton Transfer Reaction. *J. Phys. Chem. A* **2013**, *117*, 1400−1405.
(51) Barbatti, M.; Aquino, J. A.; Lischka, H.; Schriever, C.; Lochbrunner, S.; Riedle, E. Ultrafast Internal Conversion Pathway and Mechanism in 2-(2′-Hydroxyphenyl)benzothiaxole: A Case Study for Excited-State Intramolecular Proton Transfer Systems. *Phys. Chem. Chem. Phys.* **2009**, *11*, 1406−1415.